JETIR.ORG ISSN: 2349-5162 | ESTD Year : 2014 | Monthly Issue
JOURNAL OF EMERGING TECHNOLOGIES AND INNOVATIVE RESEARCH (JETIR)
An International Scholarly Open Access, Peer-reviewed, Refereed Journal

Thermal Convection in a Casson Nanofluid Layer Saturating Porous Medium: Darcy-Brinkman Model

Mamta Devi [1*], Urvashi Gupta [2]

[1]Energy Research Centre, Panjab University, Chandigarh-160014, India.
2Dr. S.S. Bhatnagar University Institute of Chemical Engineering and Technology, Panjab University, Chandigarh-160014, India.

*Corresponding author.
E-mail address: dmamta015@gmail.com (Mamta Devi).

Abstract

The convective instability of a porous layer saturating a viscoplastic Casson nanofluid is investigated analytically and numerically. Darcy Brinkman model is used to frame momentum equation for the system and non-Newtonian behavior is explored for Casson fluid. The model incorporates the diffusion coefficients due to Brownian motion and thermophoresis. Normal mode technique is used to simplify the governing equations and linear stability theory is employed. The present study finds the expressions of thermal Rayleigh number for free- free, rigid-free and rigid-rigid boundaries and discusses the effects of various parameters on the onset of convection currents in the fluid layer using the software Wolfram Mathematica. Out of all three boundaries, rigid-rigid boundaries make the fluid layer most stable. It is found that Darcy number and porosity parameter delay the onset of convection currents in the fluid layer while Casson parameter, nanoparticle Rayleigh number and Lewis number show a destabilizing influence on the system.

Keywords: Nanoparticles; Non-Newtonian fluid; Casson model; Brownian motion; Thermophoresis; Darcy Brinkman model.

Nomenclature

a	wave number	α_m	thermal diffusivity of fluid
c_p	specific heat capacity	β	Casson parameter
d	depth of the layer	β_t	thermal volumetric coefficient
D_b	Brownian diffusion coefficient	γ	conductivity variation parameter
D_t	thermophoresis diffusion coefficient	ε	porosity
e_{ij}	deformation rate	$\hat{\mu}$	effective viscosity parameter
g	acceleration due to gravity	μ_d	dynamic viscosity
k	thermal conductivity of nanofluid	τ	stress tensor
k_m	overall thermal conductivity	ρ_p	nanoparticle density

K	Permeability	ρ_0	fluid density at temperature T_0
m_x	wave number in x-pivot	$(\rho c)_m$	effective heat capacity
n_y	wave number in y-pivot	σ	thermal capacity
p	pressure	ϕ	Relative nanoparticle volume fraction $\frac{\phi-\phi_0}{\phi_1-\phi_0}$
s	growth rate	**Non-dimensional parameters**	
t	time	D_a	Darcy parameter
T	temperature	L_n	nanofluid Lewis number
T_0	temperature at upper layer	N_a	diffusivity ratio
T_1	temperature at lower layer	N_b	particle density increment
u_D	Darcy-velocity ($u=(u,v,w)$)	p_r	Prandtl number
Y_y	yield stress for Casson fluid	R_a	Darcy-Rayleigh number
(x,y,z)	cartesian co-ordinate system	R_m	basic-density Rayleigh number
z	an axis of coordinate system	R_n	nanoparticle Rayleigh number

Superscripts

^	perturbed variable
*	non-dimensional variable

Greek-symbols

1. Introduction

Nowadays, there has been a great interest in nanofluids, which are a combination of ordinary fluid with a small number of suspended metallic or non-metallic particles and resulting fluid was coined as 'Nanofluid' by Choi [1]. Nanofluids transfer heat more efficiently than the conventional fluids and are widely utilized in a variety of applications including as a coolant in automobiles, as a fuel and to minimize heat resistance in medical and electrical equipment. Buongiorno [2] made a significant contribution to nanofluid modelling by pointing out that the absolute velocity of nanoparticles is the sum of the base fluid velocity and the relative velocity. The model was further used by many researchers [3-6] to study the convective heat transfer in nanofluids and was modified by Nield and Kuznetsov [7] to consider the solutal effects on a nanofluid layer. The analytical investigations were made to establish the destabilizing impact of solute and nanoparticles on the system. Gupta et al. [8] considered a binary nanofluid layer under magnetic field. Contrary to solutal and nano scale effects, magnetic field was found to delay the convection in the layer. To consider the influence of density as well as conductivity of nanoparticles on the fluid, steady state solution for nanoparticle volume fraction was assumed to be constant [9] and the problem was studied numerically for different metallic and non-metallic nanofluids. The fluid flow through porous media has been a subject of active research due to its wide range of applications in fields of science and engineering. Nield and Kuznetsov [10] studied the thermal convection problem for nanofluids in porous medium using Brinkman model for all three boundaries (both free, rigid-free, both rigid). Rotation and magnetic field make the binary nanofluid layer more stable while porosity effects speed up the initiate the convection currents in the fluid layer [11,12]. Dhananjay et al. [13] examined the instability of a porous layer under internal heat source and both Darcy number and porosity contribute in the stability while internal heat source and nanoparticles destabilize the system.

Casson model fits well to various non-Newtonian fluids [14] such as blood, jelly, tomato sauce, honey, soup and concentrated fruit juices etc. Blood behaves like a Casson fluid in moderate shear rate flows, according to Blair and Spanner [15], thus it is reasonable to infer blood is a Casson fluid. Casson's equation's success was investigated by Scott Blair [16]. They discovered the dual nature solution for the suggested model with thermal radiation impacts on both the steady and unsteady Casson fluid flow by Hamid et al. [17]. Natural convection in a partially heated porous medium was examined by Aneja et al. [18] for Casson fluid and the penalty finite element approach was used to solve the flow problem's non-linear coupled equations. Recently, Casson model is used for various nanofluid flow problems to study the impact of nanoparticles on blood flow. Effect of variable thermal conductivity and viscosity on a boundary layer MHD Casson nanofluid flow with convective heating and velocity slip was considered by Gbadeyan et al. [19].

Casson nanofluid convection in an internally heated layer was studied by Gupta et al. [20]. Recently, Gupta et al. [21] studied double-diffusive instability of Casson nanofluids and numerical investigations were made for blood-based fluid.

Unlike the previous works, the present paper studies the phenomenon of Darcy-Brinkman convective instability in a non-Newtonian (Casson) nanofluid layer saturating porous medium. The set of partial differential equations satisfying conservation laws are converted to ordinary using normal mode technique [22] and linear stability theory is employed. These equations are solved using one term Galerkin method to find eigen value equations for free-free, rigid-free and rigid-rigid boundaries. Top layer of configuration is assumed to have less nanoparticle volume fraction as compared to lower which assures the non-occurrence of oscillatory motions [7,10]. The stationary convective instability is illustrated through graphs for critical Rayleigh number versus Casson parameter for different values of nanoparticle Rayleigh number, modified diffusivity ratio, Lewis number, Darcy number, modified particle-density increment and porosity on the stability of the system. It is found that Darcy number and porosity have stabilizing impact while Casson parameter, nanoparticle Rayleigh number, Lewis number show a destabilizing influence. Also, modified diffusivity ratio and particle density increment parameters do not have any impact on the instability of the system.

2. Governing equations for fluid flow

An infinite horizontal layer of incompressible nanofluid saturating porous medium is considered having thickness d. Also, a cartesian coordinate system (x, y, z) is chosen such that z-axis is perpendicular to the boundaries and gravity acts along the negative direction of z-axis. The boundaries of the porous layer have temperature and nanoparticles concentration as T_1 *and* ϕ_1 at lower boundary z=0 while T_0 *and* ϕ_0 at upper boundary z=d (where $T_1 > T_0$ *and* $\phi_1 > \phi_0$) (refer; Fig.1.)

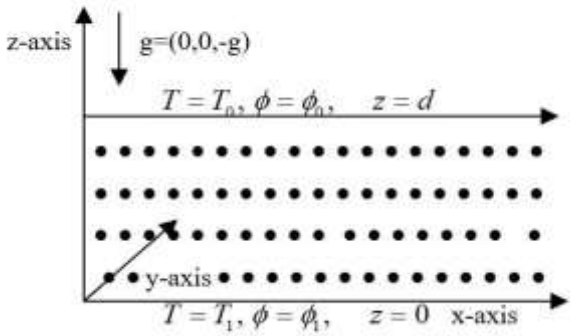

Fig. 1. Geometry of the problem.

The governing equation for Casson fluid flow (refer; [23]) is

$$\tau_{ij} = \begin{Bmatrix} \mu_d + \left(\frac{Y_y}{\sqrt{2\pi}}\right) 2e_{ij}, & \pi > \pi_c \\ \mu_d + \left(\frac{Y_y}{\sqrt{2\pi_c}}\right) 2e_{ij}, & \pi < \pi_c \end{Bmatrix}, \text{where } Y_y = \frac{\mu_d \sqrt{2\pi}}{\beta}, \tag{1}$$

and $\pi = e_{ij} e_{ij}$, $e_{ij} = \frac{1}{2}\left(\frac{\partial v_i}{\partial x_j} + \frac{\partial v_j}{\partial x_i}\right)$.

The governing equations for a Casson nanofluid layer are (refer; [2,5])

$$\nabla . u_D = 0, \tag{2}$$

$$\frac{\rho_0}{\varepsilon}\frac{\partial u_D}{\partial t} = -\nabla p + \hat{\mu}\, div\, \tau - \frac{\mu}{K} u_D + \left[\phi \rho_P + (1-\phi)\left\{\rho_0 (1-\beta_t (T - T_0))\right\}\right] g. \tag{3}$$

Using Eq. (1) in Eq. (3), we get

$$\frac{\rho_0}{\varepsilon}\frac{\partial u_D}{\partial t} = -\nabla p + (1+1/\beta)\hat{\mu}\nabla^2 u_D - \frac{\mu}{K} u_D + \left[\phi \rho_P + (1-\phi)\left\{\rho_0 (1-\beta_t (T - T_0))\right\}\right] g, \tag{4}$$

$$(\rho c)_m \frac{\partial T}{\partial t} + (\rho c)_f u_D . \nabla T = k_m \nabla^2 T + \varepsilon (\rho c)_p \left[D_b \nabla \phi . \nabla T + \frac{D_t}{T_0} \nabla T . \nabla T \right], \tag{5}$$

$$\frac{\partial \phi}{\partial t}+\frac{1}{\varepsilon}u_D.\nabla\phi = D_b\nabla^2\phi + D_t\nabla^2\frac{T}{T_0}, \tag{6}$$

Let us assume that the temperature and volumetric fractions are constant on the boundaries and hence boundary conditions become

$$\begin{aligned} &w=0, \frac{\partial w}{\partial z}+l_1\ d\ \frac{\partial^2 w}{\partial z^2}=0, T=T_1, \phi=\phi_1 \ \ at\ z=0, \\ &w=0, \frac{\partial w}{\partial z}-l_2\ d\ \frac{\partial^2 w}{\partial z^2}=0, T=T_0, \phi=\phi_0 \ \ at\ z=d, \end{aligned} \tag{7}$$

where the parameters l_1 *and* l_2 take the value ∞ for free boundaries and 0 for rigid boundaries.

Now we non-dimensionlize the variables as

$$\begin{aligned} &(x,y,z)/d=(x^*,y^*,z^*),\ t^*=t\alpha_m/\sigma d^2,\ (u,v,w)d/\alpha_m=(u^*,v^*,w^*),\ p^*=pd/\mu\alpha_m, \\ &\phi^*=(T-\phi_1)/(\phi_0-\phi_1),\ T^*=(T-T_0)/(T_1-T_0),\ \text{where } \alpha_m=k_m/(\rho c)_f,\ \sigma=(\rho c)_m/(\rho c)_f. \end{aligned} \tag{8}$$

Using Eqs. (8), Eqs. (2)-(7) (after dropping the asterisks) become

$$\nabla.u=0, \tag{9}$$

$$\frac{D_a}{P_r}\frac{\partial u}{\partial t}=-\nabla p+(1+1/\beta)D_a\nabla^2 u-u-R_m e_z+R_a T e_z-R_n\phi e_z, \tag{10}$$

$$\frac{\partial T}{\partial t}+u.\nabla T=\nabla^2 T+\frac{N_b}{L_n}\nabla\phi.\nabla T+\frac{N_a N_b}{L_n}\nabla T.\nabla T\ , \tag{11}$$

$$\frac{1}{\sigma}\frac{\partial \phi}{\partial t}+\frac{1}{\varepsilon}u.\nabla\phi=\frac{1}{L_n}\nabla^2\phi+\frac{N_a}{L_n}\nabla^2 T, \tag{12}$$

where,

$$\begin{aligned} &R_a=\rho_0 gKd\beta_t\frac{(T_1-T_0)}{\mu\alpha_m},\ L_n=\frac{\alpha_m}{D_b},\ P_r=\frac{\mu}{\rho_0\alpha_m}, \\ &N_b=\varepsilon(\rho c)_p\frac{\phi_1-\phi_0}{(\rho c)_f},\ N_a=\frac{D_t}{D_b}\frac{(T_1-T_0)}{T_1(\phi_1-\phi_0)},\ D_a=\frac{\hat{\mu}K}{\mu d^2}, \\ &R_m=(\rho_p\phi_1+\rho_0(1-\phi_1)gdK/\mu\alpha_m,\ R_n=\frac{(\rho_p-\rho_0)(\phi_1-\phi_0)}{\mu\alpha_m}gdK. \end{aligned} \tag{13}$$

And boundary conditions become for unit depth of layer are

$$\begin{aligned} &w=0, \frac{\partial w}{\partial z}+l_1\ \frac{\partial^2 w}{\partial z^2}=0, T=1, \phi=0 \ \ at\ z=0, \\ &w=0, \frac{\partial w}{\partial z}-l_2\ \frac{\partial^2 w}{\partial z^2}=0, T=0, \phi=1 \ \ at\ z=1. \end{aligned} \tag{14}$$

3. Steady state solutions and normal mode technique

Initially, the fluid layer is at rest and variables vary along horizontal axis. Thus Eqs. (9)-(12) give

$$T(z)=1-z,\ \ \phi(z)=z. \tag{15}$$

Now we add perturbations to initial solutions and write

$$u=u+\hat{u},\ p=p+\hat{p},\ \phi=\phi+\hat{\phi},\ T=T+\hat{T}. \tag{16}$$

Equations (9)-(12) with the help of Eqs. (15 and 16), give us a set of perturbed differential equations as

$$\nabla.\hat{u}=0, \tag{17}$$

$$\frac{D_a}{P_r}\left(\frac{\partial \hat{u}}{\partial t}\right) = -\nabla \hat{p} + D_a\left(1+1/\beta\right)\nabla^2 \hat{u} - \hat{u} + R_a \hat{T} e_z - R_n \hat{\phi} e_z, \tag{18}$$

$$\frac{\partial \hat{T}}{\partial t} + \hat{w} = \nabla^2 \hat{T} + \frac{N_b}{L_n}\frac{\partial \phi}{\partial z}\frac{\partial \hat{T}}{\partial z} + \frac{N_b}{L_n}\frac{\partial T}{\partial z}\frac{\partial \hat{\phi}}{\partial z} + 2\frac{N_a N_b}{L_n}\frac{\partial \hat{T}}{\partial z}\frac{\partial T}{\partial z}, \tag{19}$$

$$\frac{1}{\sigma}\frac{\partial \hat{\phi}}{\partial t} + \frac{1}{\varepsilon}\frac{\partial \hat{\phi}}{\partial z}\hat{w} = \frac{1}{L_n}\nabla^2 \hat{\phi} + \frac{N_a}{L_n}\nabla^2 \hat{T}, \tag{20}$$

Now on Eq. (18) together with Eq. (17) and using the relation $curlcurl = graddiv - \nabla^2$, we get

$$\frac{D_a}{P_r}\frac{\partial}{\partial t}\left(\nabla^2 \hat{w}\right) + \nabla^2 \hat{w} - \left(1+1/\beta\right) D_a \nabla^4 \hat{w} = R_a \nabla_H^2 \hat{T} - R_n \nabla_H^2 \hat{\phi}, \tag{21}$$

where $\nabla^2 = \frac{\partial^2}{\partial^2 x} + \frac{\partial^2}{\partial^2 y} + \frac{\partial^2}{\partial^2 z}$ and $\nabla_H^2 = \frac{\partial^2}{\partial^2 x} + \frac{\partial^2}{\partial^2 y}$ (Laplacian operators).

To use normal mode technique on Eqs. (17)-(21), let us write perturbed variables as [refer; 22]

$$\left(\hat{w}, \hat{T}, \hat{\phi}\right) = \left[W(z), T(z), \phi(z)\right](z)\exp\left(im_x x + in_y y + st\right). \tag{22}$$

Using Eq. (22) in Eqs. (17)-(21), we get

$$\left(\left(1+1/\beta\right) D_a \left(D^2 - a^2\right)^2 - \left(D^2 - a^2\right)\right) W - a^2 R_a T + a^2 R_n \phi = 0, \tag{23}$$

$$W + \left(D^2 - a^2 + \frac{N_b}{L_n}(D - 2\frac{N_a N_b}{L_n} D\right) T - \frac{N_b}{L_n} D\phi = 0, \tag{24}$$

$$-\frac{1}{\varepsilon} W + \frac{N_a}{L_n}(D^2 - a^2) T + \frac{1}{L_n}(D^2 - a^2)\phi = 0, \tag{25}$$

with $D = \frac{d}{dz}$, $a = (m^2{}_x + n^2{}_y)^{1/2}$.

The boundary conditions for both free, rigid-free and both rigid boundaries (given by Eq. (14)) reduce to

$$W = D^2 W = T = \phi = 0 \ \ at \ \ z = 0\,1, \quad for \ \ free - free \ boundaries. \tag{26}$$

$$W = DW = T = \phi = 0 \ \ at \ \ z = 0, \quad rigid \ \ boundary,$$
$$W = D^2 W = T = \phi = 0 \ \ at \ \ z = 1, \quad free \ \ boundary. \tag{27}$$

$$W = DW = T = \phi = 0 \ \ at \ \ z = 0\,1, \quad for \ both \ rigid \ \ boundaries. \tag{28}$$

Equations (23)-(25) are solved using one-term Galerkin method to get the expressions of Darcy-Rayleigh number for free-free, rigid-free and rigid-rigid boundaries given by Eqs. (26)-(28).

4. Expression of Rayleigh number (for s=0)

4.1 Free-free boundaries

If both the boundaries of the fluid layer are free then the boundary conditions can be taken as [Eq. 26]

$$W = D^2 W = T = \phi = 0 \ \ at \ \ z = 0 \ and \ \ z = 1. \tag{29}$$

Trial solutions satisfying Eq. (29) are

$$(W, T, \phi) = (L, M, N)\sin \pi z, \tag{30}$$

Using one term Galerkin method, put these trial solutions in Eqs. (23)-(25) and then solve residue integrals to get a system of equations in three unknown coefficients L, M, N. Then eigen value equation after elimination of unknowns, gives the expression for Rayleigh number as

$$R_a = \frac{2D_a(1+1/\beta)J^4 + 2J^3 - 2a^2 J L_n R_n/\varepsilon}{2a^2 J} - R_n N_a, \quad (31)$$

where $J = \pi^2 + a^2$.

4.2 Rigid-free boundaries

The boundary conditions for rigid-free boundaries are [Eq. (27)]

$$W = DW = T = \phi = 0 \quad at\ z = 0 \text{ (rigid boundary)},$$
$$W = D^2W = T = \phi = 0 \quad at\ z = 1 \text{ (free boundary)}. \quad (32)$$

The trial solutions for such boundaries are

$$W = L z^2(1-z)(3-2z),\ T = M(z-z^2),\ \phi = N(z-z^2), \quad (33)$$

Using Eq. (33) in Eqs. (23)-(25), one term Galerkin method gives the expression for Rayleigh number as

$$R_a = \frac{28[D_a\varepsilon(1+1/\beta)(4536+432a^2+19a^4)+\varepsilon(216+19a^2))](10+a^2)^2 - 507a^2 R_n L_n(10+a^2)}{507a^2\varepsilon(10+a^2)} - R_n N_a. \quad (34)$$

4.3. Rigid-rigid boundaries

Let us take the rigid-rigid boundary conditions as [Eq. (28)]

$$W = DW = T = \phi = 0 \quad at\ z = 0\ and\ z = 1. \quad (35)$$

We can write the trial solutions as

$$W = L(z^4 - 2z^3 + z^2),\ T = M(z-z^2),\quad \phi = N(z-z^2). \quad (36)$$

Equations (23)-(25) can be solved by using one-term Galerkin method for rigid-rigid boundary conditions with the help of these trial solution (Eq. (36)) and gives the expression for Rayleigh number as

$$R_a = \frac{56[D_a\varepsilon(1+1/\beta)(504+24a^2+a^4)+\varepsilon(12+a^2))](10+a^2)^2 - 54a^2 L_n R_n(10+a^2)}{54a^2\varepsilon(10+a^2)} - R_n N_a. \quad (37)$$

5. Validation of Results and Approximate Solution

5.1. Both Free boundaries

When $\beta \to \infty$ in the Rayleigh number expression in Eq. (31) matches the expression given by Nield and Kuznetsov [10]

$$R_a = \frac{D_a J^3 + J^2}{a^2} - R_n(N_a + \frac{L_n}{\varepsilon}),\ where\ \ J = \pi^2 + a^2. \quad (38)$$

Also Eq. (31) can be written as

$$R_a + R_n(N_a + \frac{L_n}{\varepsilon}) = \frac{D_a(\pi^2+a^2)^3(1+\frac{1}{\beta}) + (\pi^2+a^2)^2}{a^2}\ . \quad (39)$$

When $D_a = 0$ then $R_a + R_n(N_a + \frac{L_n}{\varepsilon}) = 4\pi^2$, that is the lowest value attained at $a = \pi$.

When $D_a = 1$ then $R_a + R_n(N_a + \frac{L_n}{\varepsilon}) = \frac{27}{4}\pi^2$, that is the lowest value attained at $a = \frac{\pi}{\sqrt{2}}$.

Therefore, using the large value of D_a as unity, critical wave number for free-free boundary is around 2.22 and critical Rayleigh number is around 657.5.

5.2. Rigid-free boundaries

Equation (34) by putting $\beta \to \infty$, provides the expression of Rayleigh number as

$$R_a = \frac{28\,[D_a(4536 + 432a^2 + 19a^4) + 216 + 19a^2](10 + a^2)}{507a^2} - R_n(\frac{L_n}{\varepsilon} + N_a), \tag{40}$$

which is same as that of Nield and Kuznetsov [10] for rigid-free boundaries. Also, Eq. (40) can be written as

$$R_a + R_n(N_a + \frac{L_n}{\varepsilon}) = \frac{28\,[D_a(1+1/\beta)\,(4536 + 432a^2 + 19a^4) + 216 + 19a^2](10 + a^2)}{507a^2}. \tag{41}$$

When $D_a = 0$ then $R_a + R_n(N_a + \frac{L_n}{\varepsilon}) = 48.01$, which is minimum value obtained at $a = 3.27$.

When $D_a = 1$ then $R_a + R_n(N_a + \frac{L_n}{\varepsilon}) = 1139$, which is minimum value obtained at $a = 2.67$.

Hence, critical wave number for rigid-free boundaries is 2.67 when D_a is large compared with unity which is also used to calculate the value of critical Rayleigh number as 1139.

5.3. Rigid-rigid boundaries

Let us take $\beta \to \infty$ in Eq. (37), we get expression of Rayleigh number

$$R_a = \frac{28[D_a(504 + 24a^2 + a^4) + (12 + a^2))](10 + a^2)}{27a^2} - R_n(N_a + \frac{L_n}{\varepsilon}). \tag{42}$$

This is the same expression given by Nield and Kuznetsov [10] for porous layer only. Eq. (41) can also be written as

$$R_a + R_n(N_a + \frac{L_n}{\varepsilon}) = \frac{28[D_a(1+\frac{1}{\beta})(504 + 24a^2 + a^4) + (12 + a^2))](10 + a^2)}{27a^2}. \tag{43}$$

When $D_a = 0$ then $R_a + R_n(N_a + \frac{L_n}{\varepsilon}) = 43.92$, which is minimum value obtained $a = 3.31$.

When $D_a = 1$ then $R_a + R_n(N_a + \frac{L_n}{\varepsilon}) = 1750$, which is minimum value obtained at $a = 3.12$.

Hence, when D_a is very large as compared with unity then critical wave number for rigid-rigid boundaries is 3.12 and critical Rayleigh number 1750 approximately.
Here, right hand side of Eq. (43) is higher than that of Eqs. (39) and (41) and hence rigid-rigid boundaries are more practical boundaries.

6. Numerical results and discussions

Let us look at the problem numerically to see how the value of critical Rayleigh number varies with Casson parameter for fixed values of different parameters using the software Wolfram Mathematica. The expressions of Rayleigh number (Eqs. (31), (34), and (37)) are dependent on multiple parameters. Let us take fixed values of parameters as follows: $L_n = 100, N_a = 1, N_b = 0.01, R_n = 0.1, D_a = 0.5, \varepsilon = 0.9$ and vary one of the variables to analyze its impact on instability of the system. Figure 2 depicts the relationship between critical Rayleigh number and Casson parameter β for various values of nanoparticle Rayleigh-number R_n with all three boundaries for fixed values of other parameters. It is noted that when nanoparticle Rayleigh number increases (increment in volumetric fraction, increases the Brownian motion of the nanoparticles), critical Rayleigh number decreases with respect to Casson parameter β and hence nanoparticle Rayleigh number has a destabilizing effect on the system. Figure 3 plots the graph of critical Rayleigh number as a function of Casson parameter β for different values of modified diffusivity

ratio N_a . One can easily observe that critical Rayleigh number for all three (rigid-free, rigid-rigid and free-free) boundaries do not get affected by increment in modified diffusivity ratio N_a and hence doesn't have any impact on the initiation of convection currents in the fluid layer system.

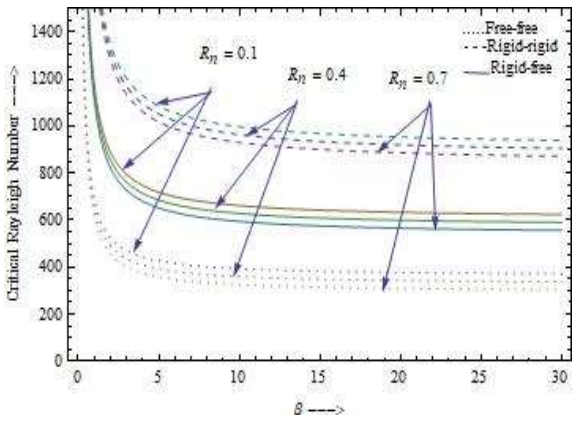

Fig. 2 Critical R_a versus β for different values of R_n.

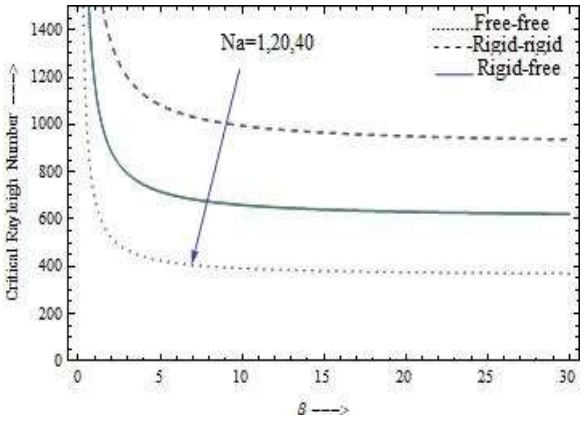

Fig. 3 Critical R_a versus β for different values of N_a.

There is no significant change in the stability curves for different values of modified particle-density increment N_b as interpreted in Fig.4 and hence doesn't have much impact on the onset of instability of the fluid layer. Figure 5 shows the stability curves of critical Rayleigh-number in the presence of Casson parameter β for different values of Lewis number L_n . It is observed that critical Rayleigh number decreases for increasing values of Lewis number and therefore a destabilizing impact of Lewis number is established for all three boundaries.

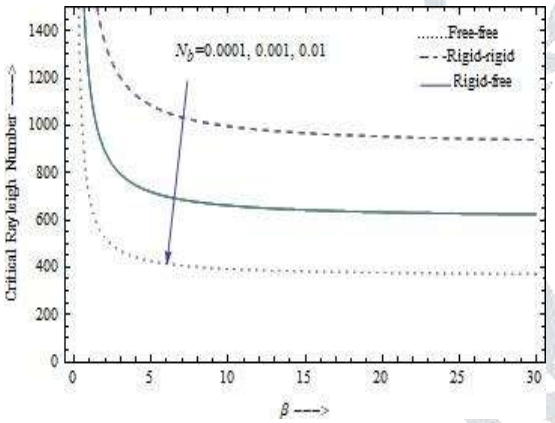

Fig. 4 Critical R_a versus β for different values of N_b.

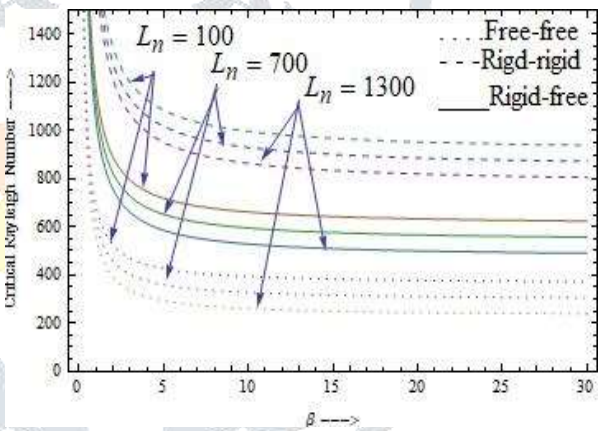

Fig. 5 Critical R_a versus β for different values of L_n.

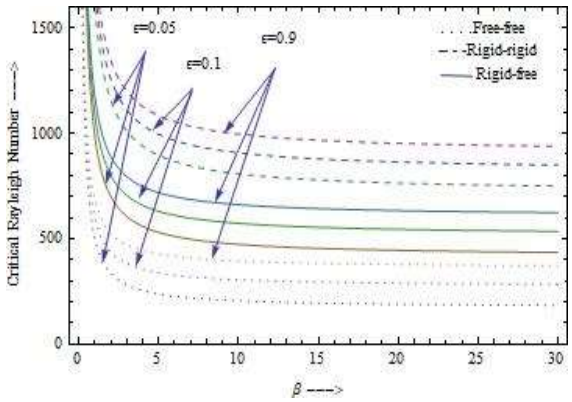

Fig. 6 Critical R_a versus β for different values of ε.

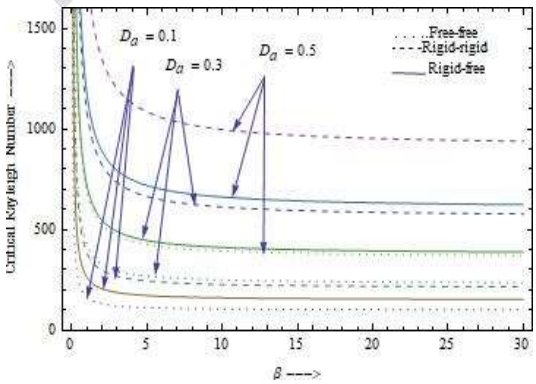

Fig. 7 Critical R_a versus β for different values of D_a.

Figure 6 depicts the effect of porosity parameter ε on critical Rayleigh number and it is noted that when porosity parameter increases, value of critical Rayleigh number also increases. So, it is indicating that porosity parameter delays the onset of convection in the nanofluids layer. Figure 7 plots the stability curves of critical Rayleigh number as function of Casson parameter β for different values of Darcy parameter. It is clear from the graph that the value of critical Rayleigh number increases with an increment in Darcy

parameter and hence it delays the onset of convection in the nanofluid layer system. The reason for this is the increment in effective viscosity with the increment in Darcy parameter which retards the fluid flow. In Figs. 2-7, for smaller values of Casson parameter, critical Rayleigh number decreases rapidly whereas for increasing values of β doesn't show much variation in its values.

To know the effect of Darcy parameter more efficiently, let us plot the graphs of $\log D_a$ versus critical Rayleigh number R_{a_c} and $\log D_a$ versus critical wave number a_c. Here, one can observe that the values of R_{a_c} increases when Darcy parameter increases in Fig. 8 and hence has a stabilizing effect on the system. Figure 9 shows that when Darcy parameter increases, critical wave number decreases which leads to increase in the size of convection cells and hence delays the onset of convection.

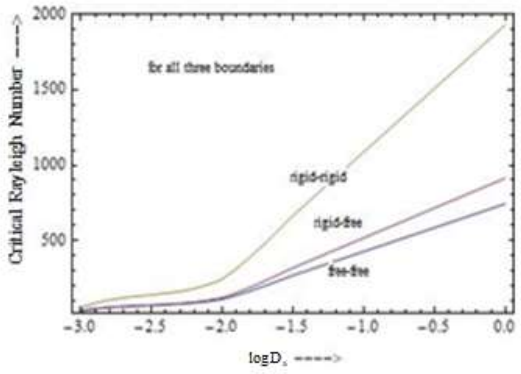

Fig. 8 Critical R_a versus $\log D_a$.

Fig. 9 Critical a_c versus $\log D_a$.

Fig. 10 Critical wave number a_c versus β.

Effect of Casson parameter β on critical wave number a_c is shown in Figure 10. It is observed that the value of critical wave number a_c doesn't vary much with the variation in Casson parameter β and only small values of Casson parameter has a slight effect on the value of critical wave number. Thus, non-Newtonian behaviour largely doesn't show any impact on critical wave number.

Interestingly, in all the figures the critical Rayleigh number for rigid-rigid boundaries is greater than that of rigid-free boundaries, which is more than that of free-free boundaries and thus the system is the most stable for realistic rigid-rigid boundaries.

7. Conclusions

The convective instability of a non-Newtonian nanofluid layer under Casson model is investigated analytically and numerically using Darcy-Brinkman model. Normal mode technique is used to convert partial differential equations into ordinary and linear stability theory is employed. The obtained set of ordinary differential equations are solved using one term Galerkin method to find an eigen value equation for free-free, rigid-free and rigid-rigid boundaries. Effect of Casson parameter on critical Rayleigh number for different values of nanoparticle Rayleigh number, modified diffusivity ratio, Lewis number, Darcy number, modified particle-density increment and porosity on the stability of the system are illustrated graphically using the software Mathematica. It is found that critical wave number for rigid-rigid boundaries are higher than that of rigid-free and free-free boundaries and critical wave number is independent of nanoparticle Rayleigh number, modified diffusivity ratio and Lewis number. It is found that Darcy number and porosity have stabilizing effect on the system while other nanofluid parameters show a destabilizing effect on the fluid layer. Modified diffusivity ratio and particle density increment parameters do not show much impact on the onset of convection currents in

the system. Non-Newtonian property (Casson parameter) destabilizes the system significantly for small values of Casson parameter which otherwise doesn't show much influence on the stability of the fluid layer. Out of all three boundaries, the system is found to be most stable for realistic rigid-rigid boundaries.

Declaration of Competing Interest: The authors declare that they have no known competing financial interests or personal relationships that could have appeared to influence the work reported in this paper.

Acknowledgements: One of the authors, Mamta Devi is thankful to Council of Scientific and Industrial Research, New Delhi-110012, India for the financial assistance in the form of SRF [Ref. No.: 09/135 (0895)/2019-EMR-I].

References

[1] Choi, S. U. S., Eastman J. A., Wang H.P. (Eds), 1995: Enhancing thermal conductivity of fluid with nanoparticle, *Development and Application of Non-Newtonian flow. ASME FED- 231/MD*-66, 99-105.

[2] Buongiorno, J., 2006: Convective transport in nanofluid. *ASME J. Heat transfer*. 128, 240-250.

[3] Tzou D. Y., 2008: Instability of nanofluids in natural convection, *ASME J. Heat Trans*. 130, 1-9.

[4] Tzou D. Y.: Thermal instability of nanofluids in natural convection, *Int. J. Heat Mass Transf*. 51, 2967-79.

[5] Yadav, D., Agrawal, G. S., Bhargava, R., 2011: Rayleigh-Benard convection in nanofluid. *Int J. Appl. Math. Mech*. 7(2), 61-76.

[6] Nield, D.A., and Kuznetsov, A.V., 2010, "The Onset of Convection in a Horizontal Nanofluid Layer of Finite Depth," *Euro. J. Mech. B/Fluids, 29, pp. 217-223.*

[7] Nield, D. A., Kuznetsov, A. V., 2011: The onset of double-diffusive convection in a nanofluid layer. *Int. J. Heat and Fluid Flow*. 32(4), 771-776.

[8] Gupta, U., Sharma, J., Sharma, V.,2015: Instability of binary nanofluid with magnetic field. *Appl. Math. Mech*. 6, 693-706.

[9] Sharma, J., Gupta, U., and Sharma, V., 2017: Modified model for binary nanofluid convection with initial constant nanoparticle volume fraction. *J. Appl. Fluid Mech*. 10, 1387-95.

[10] Nield, D. A., Kuznetsov, A.V., 2010: Thermal instability in a porous medium layer saturated by a nanofluid: Brinkman Model. Trans. Porous Med. 81(13), 409-422.

[11] Sharma, J., Gupta, U., and Wanchoo, R. K., 2016: Numerical study on binary nanofluid convection in a rotating porous layer. *Differ. Equ. Dyn. Syst, doi.org/10.1007/s12591-015-0268-4.*

[12] Sharma, J., Gupta, U., and Wanchoo, R. K., 2016: Magneto binary nanofluid convection in porous medium. *Int. J. Chem. Engi., 2016, 9424036.*

[13] Yadav, D., Agrawal, G. S., Bhargava, R., 2012: Boundary and internal heat source effects on the onset of Darcy-Brinkman convection in a porous layer saturated by nanofluid. *Int J. Therm. Scie. 60, 244-254.*

[14] Copley, A. L., 1960: Apparent viscosity and wall adherence of blood systems, in Flow Properties of Blood and Other Biological Systems, 97-121.

[15] Scott Blair G. W., 1959: An equation for the flow of blood, plasma and serum through capillaries. Nature, 183, 613-614.

[16] Scott Blair, G. W., 1966: The success of Casson's equation. Rheol. Acta sep. 5(3), 184-187.

[17] Hamid, M., Usman, M., Khan, Z. H., Ahmad, R., Wang, W., 2019: Dual solutions and stability of flow and heat transfer of Casson fluid over a stretching sheet. Phys. Lett. A. 383, 2400-2408.

[18] Aneja, M., Chandra, A., Sharma, S., 2020: Natural convection in a partially heated porous cavity to Casson fluid, Int. Commun. Heat Mass Transf. 114, 1045555.

[19] Gbadeyan J. A., Titiloye E. O., Adeosun A. T., 2020: Effect of thermal variable conductivity and viscosity on Casson nanofluid flow with convective heating and velocity slip. *Heliyon*. 6, e03076.

[20] Gupta U., Sharma J., Devi M., 2020: Casson nanofluid convection in an internally heated layer. *Mater. Today Proc*. 28, 1748-52.

[21] Gupta U., Sharma J., Devi M., 2021: Double-diffusive instability of Casson nanofluids with numerical investigations for blood-based fluid. *Eur. Phys. J. Spec. Top*. 9 (2021), https://doi.org/1.1140/epjst/s11734-021-00053.

[22] Chandrasekhar S. 1981: *Hydrodynamic and Hydromagnetic Stability, Dover Publications, New York, USA.*

[23] Mehmood, S., Nawaz, M., Ali, A., 2018: Finite volume solution of non-Newtonian Casson fluid flow in a square cavity. *Commun. Math. Appl*. 9(3), 459-474, https://doi.org/10.26713/cmav9i3.795.